J. Fluid Mech. (2000), *vol.* 417, *pp.* 77–102. Printed in the United Kingdom

Saltation and incipient suspension above a flat particle bed below a turbulent boundary layer

By K. NISHIMURA[1] AND J. C. R. HUNT[2,3]

[1]Institute of Low Temperature Science, Hokkaido University, Japan

[2]Department of Space and Climate Physics, and Geological Sciences, University College, Gordon Street, London WC1H 0AH

[3]J. M. Burges Centre, University of Technology, Delft, The Netherlands

(Received 10 May 1999 and in revised form 10 March 2000)

Experiments were conducted in a wind tunnel in which a turbulent boundary layer was naturally grown over flat beds of three types of nearly mono-disperse spherical particles with different diameters, densities and coefficient of restitution (r) (snow, 0.48 mm, 910 kg m^{-3}; mustard seeds, 1.82 mm, 1670 kg m^{-3}, $r = 0.7$; ice particles, 2.80 mm, 910 kg m^{-3}, $r = 0.8$–0.9). The surface wind speeds (defined by the friction velocity u_*) were varied between 1.0 and 1.9 times the threshold surface wind speed (defined by u_{*t}). The trajectories, and ejection and impact velocities of the particles were recorded and analysed, even those that were raised only about one diameter into the flow.

Measurements of the average horizontal flux of saltating particles per unit area, $f(z)$, at each level z above the surface showed that, for $u_*/u_{*t} \leqslant 1.5$, $f(z)$ is approximately independent of the particle density and decreases exponentially over a vertical scale length l_f, that is about 3 to 4 times the estimated mean height of the particle trajectories $\langle h \rangle$. Numerical simulations of saltating grains were computed using the measured probabilities of ejection velocities and the mean velocity profile of the air flow, but neglecting the direct effect of the turbulence. The calculated mean values of the impact velocities and the trajectory dimensions were found to agree with the measurements in the saltation range, where $u_*/u_{*t} < 1.5$. Similarly, in this range the simulations of the horizontal flux profile and integral are also consistent with the measurements and with Bagnold's u_*^3 formula, respectively.

When $u_*/u_{*t} \geqslant 1.5$, and $u_*/V_T \geqslant 1/10$, where V_T is the settling velocity, a transition from saltation to suspension occurs. This is indicated by the change in the mean mass flux profile which effectively becomes uniform with height (z) up to the top of the boundary layer. An explanation is provided for this low value of turbulence at transition relative to the settling velocity in terms of the random motion of the particles under the action of the turbulence when they reach the tops of their parabolic trajectories. The experiments show that, as u_*/u_{*t} increases from 1.0 to 1.9 the normalized mean vertical impact velocity $\langle V_{3I} \rangle/u_*$ decreases by nearly 60% to about 0.6, which is less than 50% of the value for fluid particles. There is also a decrease in the vertical and horizontal component of the ejection velocity to values of 0.8 and 2.3, which are much less than their values in the saltation regime. We hypothesize that at the transition from saltation to suspension the ejection process changes quite sharply from being determined by impact collisions to being the result of aerodynamic lift forces and upward eddy motions.

1. Introduction

Bagnold (1941) defined three transport modes for sand: saltation, suspension and surface creep. Generally once the wind speed over the grain surface is great enough for particles to enter the air stream they move up and down parabolic trajectories by a process called 'saltation' and then collide with particles on their return to the bed. He introduced two wind velocity thresholds: the impact threshold and the fluid threshold. The impact threshold is the wind velocity that must be exceeded for saltation to be maintained, whereas the fluid threshold is the wind velocity that must be exceeded for saltation to be initiated. The fluid threshold is generally thought of as being greater than the impact threshold. At higher wind speeds the particles are transported upwards by turbulent eddies and by this means can be transported far downwind of the bed. This is the process of 'suspension'. Although Bagnold used 'surface creep' to describe grains rolling and jostling along the surface, it has been redefined and renamed 'reptation', describing grains which make short hops just above the surface, having been ejected by a saltating particle.

Bagnold (1941) also identified four distinct subprocesses in the sand saltation system: aerodynamic entrainment, the grain trajectory, the grain/bed collision and wind modification. In the past decade some progress has been made in the modelling of aeolian particle transport, especially for the first three of these mechanism (Anderson & Haff 1988, 1991; Werner 1990; Sorensen 1991; McEwan & Willetts 1991), but there are still significant quantitative uncertainties in these models, which we consider in this paper. Note that although most reports have been applied to saltation over level surfaces, it appears that the results also apply on surfaces of moderate slopes such as the upwind slopes of sand dunes (e.g. Weng *et al.* 1991).

The essence of saltation is the connection between how the particles ejected into the flow are accelerated, and how, on their impact with the bed, particle–particle collisions lead to ejection of particles into the flow. Anderson (1989) described saltation in terms of an analogy with a biological population. In this analogy the wind is represented by a fixed food resource and, just as a biological population has an age distribution, so a saltation cloud contains a spectrum of trajectory lengths and duration. On impact these trajectories may eject (give birth to) other grains or may terminate (die) on colliding with the bed. Thus the grain/bed collision has a crucial role in regulating the flux of sand leaving the surface and hence in establishing the properties of the sand transport system. In addition to a computer simulation in which a solid body hits a bed of other solid bodies (Anderson, Sorensen & Willetts 1991), wind tunnel experiments have been carried out to deepen our understanding of the interaction between the impacting particles and the particles in the bed. Willetts & Rice (1985) have made the most detailed study hitherto of how an impacting sand particle leads to the ejection of several others in different directions and at several particle diameters removed from the impact spot. Nalpanis, Hunt & Barrett (1993) measured ejection and impact velocities, trajectory lengths and maximum rise heights of sand grains in saltation over a flat sand bed in a wind tunnel by digitizing multiple-image photographs. These data were shown to be consistent with those of other published experiments, including those with snow by Araoka & Maeno (1981).

In this study, we carried out wind tunnel experiments with snow particles, ice particles that were about five times the size of average snow particles, and mustard seeds, whose density is about 1.8 times larger than snow and ice. In the case of the ice particles, their trajectories were measured at three different wind speeds. We also examined the solid impact properties of the particles, because recent experimental studies by physicists (Hansen 1998) of randomly moving solid particles in air have

Material	Mean diameter (mm)	Standard deviation (mm)	Density ($kg\,m^{-3}$)	Coefficient of restitution r	Comments
Snow	0.48	0.24	910	–	–
Ice particles	2.80	0.30	910	0.8–0.9	spherical
Mustard seeds	1.80	–	1670	0.7	nearly spherical

TABLE 1. Properties of materials tested.

shown that if they are not quite ideal, for example if they have a restitution coefficient less than 0.93, their statistical patterns are radically changed and they form into clumps.

From the measurements of the ejection velocities of the particles and the mean wind speed profile, the horizontal flux profiles were computed, and compared with our measurements. This should be a good test of the existence of saltation. For the higher wind speeds when, as expected, the test fails, we examine the changes in the velocity statistics of the particles as they move randomly under the influence of turbulence in a state of 'suspension', and examine whether they continue to be ejected from the surface as a result of collisions between impacting particles and those in the bed, or whether their movements are determined more by random aerodynamic forces acting on them caused by their motion through the flow and by the turbulent eddies. We compare our results with previously proposed scaling laws for the transition between saltation and suspension.

2. Experimental equipment and procedure

2.1. *Particles used in the experiments*

In order to investigate the effect of the size and density of particles on the saltation trajectory snow, ice particles and mustard seeds were used. Their relevant properties are listed in table 1.

2.1.1. *Snow*

The snow used in the experiments was natural fine-grained snow, which was collected from outside in winter and kept in a cold room at $-10^{\circ}C$ for about a year to make the particle size more uniform and the shape more round through the vapour transport working to reduce the surface energy. Figure 1 shows the cumulative size distribution; it is approximately normal. The average particle size expressed as a diameter of a circle with equivalent projected area was 0.48 mm.

2.1.2. *Ice particles*

The ice spheres were made by dropping water droplets from injectors and freezing them in a bath of liquid nitrogen. The particles were sieved to give a uniform average diameter of 2.8 mm, about five times the size of average snow particles, with a standard deviation of 0.3 mm, as shown in figure 1. The degree of sphericity of an ice particle, defined as the ratio of the perimeter of the circle equivalent to the projected area of the particle to that of its projection, was almost unity (1.03 ± 0.02), indicating that the samples thus formed can be approximated as spheres.

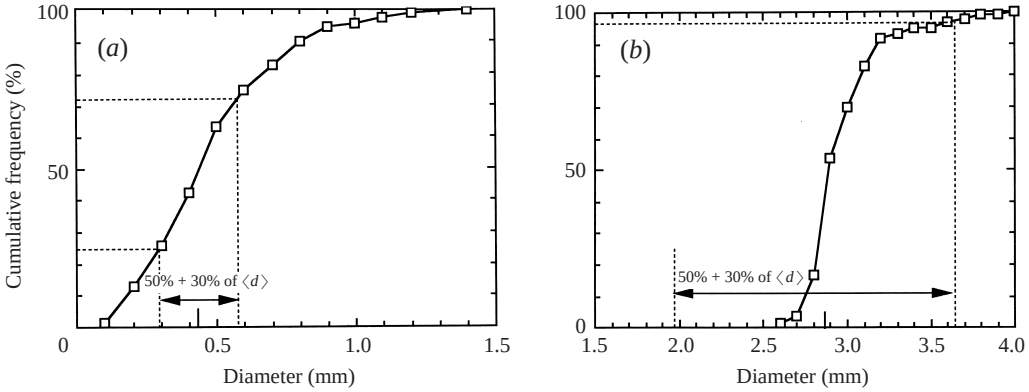

FIGURE 1. Cumulative particle size distribution: (*a*) snow, (*b*) ice particles. $\langle d \rangle$ is the mean diameter.

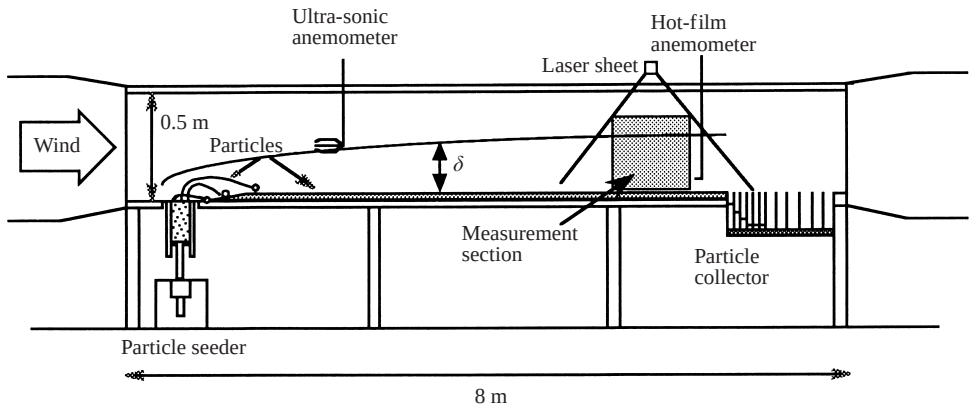

FIGURE 2. Schematic view of the cold wind tunnel at the Institute of Low Temperature Science, Hokkaido University. δ is the thickness of the boundary layer.

2.1.3. *Mustard seeds*

The mustard seeds were 1.8 mm in diameter with a narrow size distribution and can be regarded as spheres. The particle density was $1670\,\mathrm{kg\,m^{-3}}$ which is about 1.8 times larger than that of the snow and ice. The restitution coefficient of the mustard seeds (r) determined on a flat steel surface was 0.68 ± 0.13, which is about 20% smaller than the value for ice spheres (0.8–0.95) obtained by Araoka & Maeno (1978) on an ice surface.

2.2. *The wind tunnel*

A set of saltation experiments was performed in a cold wind tunnel located at the Institute of Low Temperature Science, Hokkaido University, shown schematically in figure 2. It is a closed-circuit wind tunnel situated in a large cold laboratory and has a working section of $0.5\,\mathrm{m} \times 0.5\,\mathrm{m}$ and up to 8 m in length, depending on experimental requirements. In this experiment the wind speed was varied between 7 and $13\,\mathrm{m\,s^{-1}}$. The upwind turbulence is negligible.

The temperature of the wind tunnel could be varied between 0 and −30°C, but the experiments on snow and ice particle saltation were conducted at −18°C in order to prevent rapid adhesion, by the process of sintering, between particles during the experiment; the mustard seed experiments were carried out at room temperature.

The particles used in each experiment were placed on the wind tunnel surface, forming a layer roughly 2 cm thick. The surface of the bed was prepared to be as smooth as possible. In order to initiate the saltation and maintain it steadily, seed particles of the same type as in the bed were supplied, with a device consisting of a motor-driven sieve and a screw jack as shown in figure 2, from the bottom of the wind tunnel entrance at a constant rate which corresponds to around 10% of the total saltation flux. Although seed particles have occasionally been supplied from the top of the wind tunnel in other experiments, we did not follow this method because it might change the steady uniform wind above the boundary layer. During the experiments, no surface ripples were ever observed on the surface of the bed.

2.3. *Wind velocity*

A wind tunnel reference velocity was measured with a micro ultra-sonic anemometer with a probe span of 5 cm and a time resolution of 20 Hz. It was installed on the centreline and at mid-height of the tunnel, 25 cm above the surface.

The vertical wind velocity profile in the wind tunnel was measured with a hot-film anemometer. A steady wind velocity profile was formed roughly 0.5 m downstream from the edge of the particle bed (Kosugi, Nishimura & Maeno 1992). The thickness of the steady turbulent boundary layer determined from the wind velocity profile was about 0.2 m. In the saltation cloud, impacting and melting of snow or ice particles on the probe sometimes produced significant noise on the record, and so the velocity profile in the saltation layer was obtained only in the experiment with mustard seeds. All the data were recorded by an analogue data recorder. Although too shallow wind tunnels have led to serious errors in u_* and incorrect interpretations (Owen & Gillette 1985), the depth of the tunnel (0.5 m) used in this study was sufficient compared with the depth of the boundary layer (0.2 m) and the layer of saltating particles (0.1 m). The effect of the small variation in the mean velocity profile was not expected to affect the results. After the transition to suspension, when the particles fill the boundary layer, the initial height of the boundary layer becomes more significant (see § 5).

2.4. *Particle movement*

Trajectories of saltating particles near the bed were recorded with a video system from the side of the wind tunnel. The illumination source was a laser sheet with maximum power of 2 W, which provided a vertical plane of light about 1 cm wide in the observation region. This was narrow enough to prevent particles from obscuring each other in any one image, but wide enough to enable complete trajectories to be identified. In order to interrupt the light at regular intervals, a rotating shutter with adjustable speed was applied to the laser source. Thus particle trajectories were shown as a series of dashes rather than as continuous lines (see figure 3).

The pictures obtained were digitized with a microcomputer system through the Time Base Corrector (TBC). Here, TBC was utilized as a field memory, which allowed us to capture individual field images 1/60 s apart. Thence, using the image analysis system on the microcomputer, saltation trajectory statistics, such as ejection and impact velocities, were calculated.

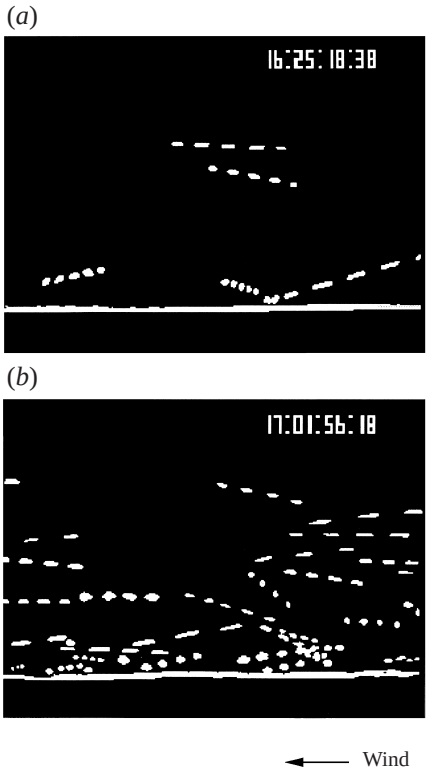

FIGURE 3. Snapshots of ice particle saltation experiments. The exposure time is 1/60 s and the frequency of illumination is 250 Hz. (*a*) $u_* = 0.50\,\mathrm{m\,s^{-1}} \approx 1.4u_{*t}$, (*b*) $u_* = 0.65\,\mathrm{m\,s^{-1}} \approx 1.9u_{*t}$.

Note that in evaluating the statistics of the trajectories of saltating particles it is necessary to distinguish them from particles that only just leave the surface. These low-level excursions up to a height h that is comparable with their diameters are largely caused by sliding and rolling collisions between particles and differ from the higher elevation trajectories of saltating particles ejected into the air flow for a sufficient distance that they are accelerated by it. Their ejection is caused by the collisions between impinging particles and those in the bed.

In this, unlike previous experiments, the particle trajectories were observed sufficiently close to the surface that it was possible to distinguish between these two types of trajectory.

For the elevated trajectories it is also necessary to distinguish between those having a random element in their form because they are affected by the turbulent eddies and those with a parabolic form that are only affected by the mean flow profile. The former are in a state of transition between saltation and suspension, while the latter are saltating (Nalpanis 1985; Bagnold 1941). Some non-parabolic trajectories are caused by the relatively rare event of particles colliding. It is clear in the image shown in figure 3(*b*) that some of the particles are indeed departing from saltation trajectories, as a result of collisions with other particles and/or interaction with turbulent eddies. Note that on several occasions, in the case where $u_*/u_{*t} = 1.9$, particles appeared to lift from the bed without any collision.

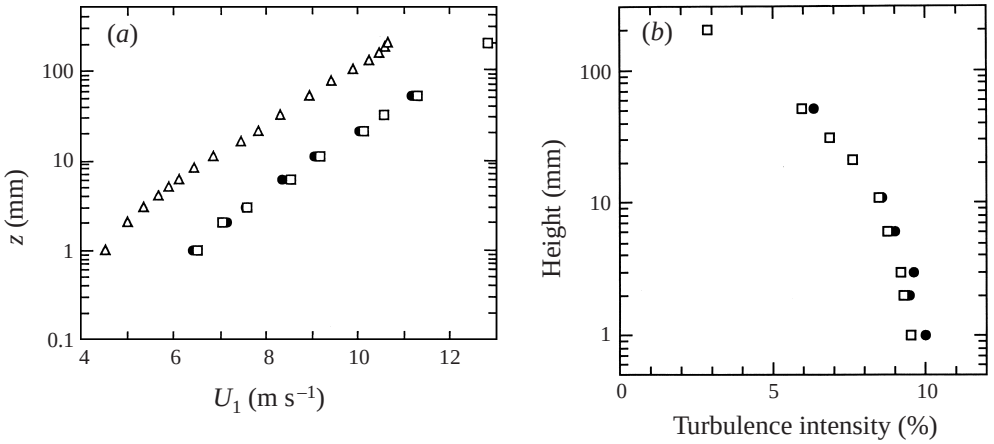

FIGURE 4. (*a*) Mean wind velocity profiles $U_l(z)$ over the mustard seed bed. No saltation: △, $u_* = 0.39\,\mathrm{m\,s^{-1}} = 1.0u_{*t}$; □, $u_* = 0.51\,\mathrm{m\,s^{-1}} \approx 1.3u_{*t}$. Saltation: ●, $u_* = 0.51\,\mathrm{m\,s^{-1}} \approx 1.3u_{*t}$. (*b*) Turbulence intensity profiles over the mustard seed bed. $u_* = 0.51\,\mathrm{m\,s^{-1}} \approx 1.3u_{*t}$: □, no saltation; ●, saltation.

3. Analysis and results

3.1. *Wind velocity*

3.1.1. *Threshold of particle motion*

When the mean wind speed $U(z)$ is plotted against the logarithm of height, as in figure 4(*a*), it is found that in the surface layer the logarithmic law of the wall applies and can be plotted as

$$U(z) = \frac{u_*}{\kappa} \ln\left(\frac{z}{z_l}\right), \tag{3.1}$$

for a distance of at least 100 mm above the bed. Here z_l is the empirically determined surface length scale where the wind velocity is zero and κ is von Kármán's constant (= 0.4). Using (3.1), the value of u_* is obtained from the slope of the plotted line. The value of z_l defined in (3.1) is only equal to the roughness length z_0 if the viscous sublayer (whose thickness $\sim 5\nu/u_* \sim 0.5$ mm in this case where ν is the kinematic viscosity of air) near the surface is thinner than z_l (i.e. $5\nu/u_* < z_l$). In this case z_l, calculated from figure 4 and the formula (3.1), varies between 0.1 and 0.01 mm. Thus, as in Nalpanis *et al.* (1993), the turbulent surface layer is hydraulically smooth. It is expected that if $z_0 > 5\nu/u_*$, then z_0 is proportional to the diameter of the particles. In the atmospheric boundary layer over blowing sand, Bagnold (1941) showed that the profile (3.1) has a different form and z_l needs to be redefined.

In this study u_* was derived from the wind speed measurements taken lower than 10 cm above the surface. This avoids any effect of Coles' wake region in the higher region of the boundary layer considered by Owen & Gillette (1985) and Janin & Cermak (1988). The velocity profiles in the saltation layer are not measurably affected by the reduction in fluid stress due to the grain cloud (Spies, McEwan & Butterfield 1995).

The threshold of particle motion is defined in terms of the friction velocity u_* of the air flow, because this enables the results of wind tunnel studies to be related to atmospheric surface processes, even though the upper part of the wind tunnel boundary layer differs from that in the atmosphere (Jensen & Franck 1965). Provided

Material	Diameter (mm)	Fluid threshold $u_{*_{tf}}$ (Bagnold's formula) ($m\,s^{-1}$)	Impact threshold u_{*_t} (measurement) ($m\,s^{-1}$)	Terminal fall speed in still air, V_T ($m\,s^{-1}$)
Snow	0.48	0.21	0.20	2.1
Ice particles	2.80	0.50	0.35	9.0
Mustard seeds	1.80	0.54	0.39	9.4

TABLE 2. Threshold of particle motion.

the processes of interest lie within the logarithmic part of the boundary layer, the only relevant length scale for comparing with full-scale data is the distance z above the surface, and the depth of the boundary layer h does not need to be considered. Of course this is an approximation, and there are effects at the surface caused by turbulence in the upper part of the boundary layer (especially at very high Reynolds number). These are discussed in § 5.

As described briefly in § 1, Bagnold (1941) found that there were two distinct threshold friction velocities for sand movement, depending on how it is initiated. In the first case, as the friction velocity increases, a threshold is reached above which grains begin to roll and hop over the surface. He used the term fluid threshold $u_{*_{tf}}$ for the lowest friction velocity at which the wind had sufficient traction on the surface to move grains. Subsequently, saltation begins when particles move vertically into the air by a distance of the order of their diameter. This is caused by collision and by aerodynamic forces. Secondly, the surface is impacted by particles of the same type as those in the bed; this bombardment produces movement at a somewhat lower (impact) friction velocity than the fluid threshold; it is typically less than the fluid threshold by a factor of 0.7–0.8. This second value of u_{*t}, can be obtained if in the first case the friction velocity is decreased, after the first type of saltation has been initiated – a type of hysteresis.

Bagnold (1941) measured the two types of fluid and impact threshold friction velocity, $u_{*_{tf}}$ and u_{*t}, for sand as a function of grain diameter. He expressed the results as

$$(u_{*_{tf}}, u_{*t}) = (A_{tf}, A_t)\sqrt{\frac{\rho\, g d}{\rho_a}}, \tag{3.2}$$

where ρ and d are the density and diameter of the particle, and ρ_a is the air density. His physical argument that aerodynamic drag moves the particles over each other suggests that $A_{tf} \sim 1/\ln(d/z_1) \ll 1$. Because of the shear profile A_{tf} decreases slightly as the particle size increases. His measurements show that for particles larger than about 200 μm, A_{tf} is 0.1. For the particles we have used in this study, the threshold velocities given by Bagnold are listed in table 2.

We have also listed the terminal fall speed V_T, which for large particles is approximately equal to $(3\rho_p g d/\rho_a)^{1/2}$, because (3.2) implies that $u_{*t} \sim V_T/17$. We return to this point in § 5. In this study, only measurements of u_{*t}, the impact threshold value of u_* on the bed, were made by visual observation. Results are shown in table 2. It is evident that the impact threshold for snow is nearly equal to the fluid threshold calculated by (3.2). However, the measured impact thresholds for ice particles and mustard seeds were about 70% of the fluid threshold, which is similar to the 80% reduction observed by Bagnold for sand particles with 250 μm diameter. This difference in the value of A_t may be caused by the fact that the equation takes no account of

particle cohesion. Snow has a wide particle size distribution, including small particles less than 100 μm, which are strongly affected by cohesive forces (Iversen & White 1982). In addition, the effects of the sintering process between particles are inevitable even at temperatures as low as −15°C. The only way to overcome these effects may be lift forces, especially those associated with bursts of turbulence (Absil & Beugeling 1984). We note that, as in (3.2), u_{*t} decreases as d increases from 1.80 mm for the mustard seeds to 2.80 mm for the ice particles.

3.1.2. *Wind speed profile in the saltation layer*

The velocity profile in the saltation layer was measured only in the mustard seed experiments, because impacting and melting of snow or ice particles on the hot film anemometer probe produced significant noise on the record and precise data were difficult to obtain.

The mean wind profiles were measured for $u_* = 39\,\mathrm{cm\,s^{-1}}$ and $51\,\mathrm{cm\,s^{-1}}$, the latter being larger than the impact threshold value of u_* but smaller than the fluid threshold; thus to generate saltation, seed particles had to be supplied, in our case from a source upwind of the bed at the bottom of the wind tunnel (see figure 2). Wind profiles obtained both before and after the initiation of saltation, in figure 4(*a*), show that without saltation the vertical velocity profile is the same as that of a turbulent boundary layer on an aerodynamically smooth surface. When saltation starts, a slight departure from the previous log profile is found. The wind speed decreased slightly above 3 mm, whereas it increased very close to the surface. Wind modification in the experiment shown in figure 4(*a*) was fairly small, perhaps because the wind speed was lower than the fluid threshold and the particle concentration was rather small. However, the modification observed here was practically the same as found by other investigators (Rasmussen, Sorensen & Willetts 1985; Maeno *et al.* 1979).

The form of the wind profile is determined by the momentum transport. Without saltation, momentum is transported by the turbulence from the wind to the bed surface. When saltation is present, momentum is also exchanged with the airborne particles, thereby accelerating them; this process produces an increased drag on the wind and a decrease in the velocity profile with an effective roughness (Owen 1964). However, the question of how much, if at all, the velocity profile is modified in the saltation layer when u_* is more than double u_{*t} continues to be controversial (e.g. McEwan & Willetts 1991; Anderson & Haff 1991) (see § 5).

Note that the turbulence level characterized by σ_*, the standard deviation of the wind velocity, is approximately equal to $2u_*$ near the surface. (Townsend 1976 explains why this is less than the value of 2.5 found in higher Reynolds number boundary layers, such as the atmospheric surface layer.) This was measured over the bed of mustard seeds when $u_* = 51\,\mathrm{cm\,s^{-1}}$. The turbulent intensity defined by $\sigma_*/U(z)$, without saltation, was about 9.5% at $z = 1$ mm above the bed surface, and decreased to 4.5% at $z = 100$ mm (figure 4*b*). When saltation was initiated with seeding particles, it increased near the surface only by 10%.

3.2. *Particle trajectories*

Trajectories of the three different types of particles were studied and their statistical results are tabulated in tables 3 and 4. For the snow particles 384 trajectories were measured at a single value of $u_* = 0.3\,\mathrm{m\,s^{-1}}$, which was 1.5 times larger than the impact threshold ($u_{*t} = 0.2\,\mathrm{m\,s^{-1}}$). For the larger mustard seed particles, 269 trajectories were measured at $u_* = 0.65\,\mathrm{m\,s^{-1}}$ (about 1.2 times the value of u_{*t}). For the even larger ice particles, 81, 370, 380 trajectories were measured for three different

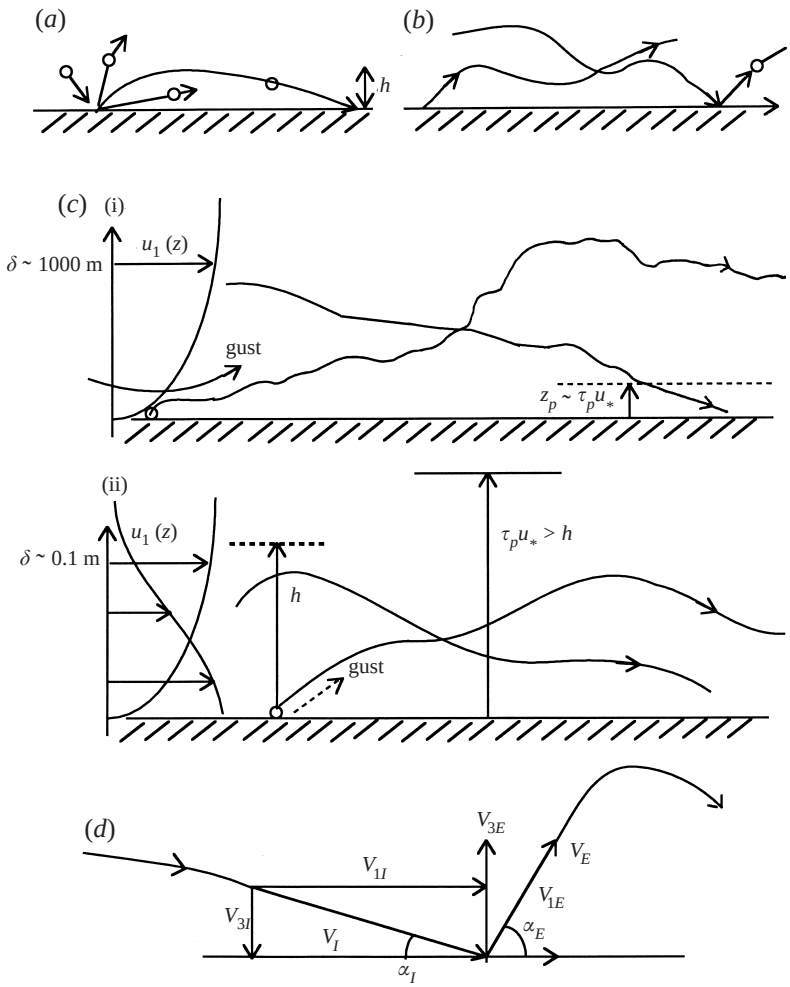

FIGURE 5. Schematic view of the process from saltation to suspension: (*a*) saltation, (*b*) modified saltation, (*c*) suspension of monodisperse particles (i, deep boundary layer; ii, laboratory boundary layer), and (*d*) the definition of quantities which characterize saltation trajectories.

value of u_* ($0.35, 0.50, 0.65\,\mathrm{m\,s^{-1}}$) corresponding to 1.0, 1.4 and 1.9 times the value of u_{*t}. Quantities which characterize the saltation paths are shown in figure 5.

In tables 3 and 4 the ejection and impact statistics are provided in dimensional and non-dimensional form, and are also compared with previous studies by Willetts & Rice (1985) (WR), White & Schulz (1977) (WS), Araoka & Maeno (1981) (AM) and Nalpanis *et al.* (1993) (NHB). Note that there are only two cases where $u_*/u_{*t} > 1.5$, the ice particles in our experiment and the glass spheres of WS. We discuss these cases separately later. In all cases the concentrations of the particles are small.

Our mean ejection angles $\langle \alpha_E \rangle$ of 25° (±15°) for snow, 23° (±18°) for mustard seeds, and 21° (±15°) for ice particles (at $u_* = 0.65\,\mathrm{m\,s^{-1}}$) are very similar to each other and are at the low end of the ranges of values 21° to 49° obtained by other investigators. This angle is particularly sensitive to how many of the low particles are counted as explained in § 2.4. Note that this angle is much less than the 90° suggested by Bagnold (1941) and assumed by Owen (1964).

	Diameter (mm)	u_* ($m\,s^{-1}$)	u_*/u_{*t}	ρ ($kg\,m^{-3}$)	Fall speed V_T ($m\,s^{-1}$)					
Snow (AM)	0.20	0.3	1.5	910	0.9					
Sand (WR)	0.15–0.60	0.39	[1.3–2.6]	2650	1.3–5.3					
Sand (NHB)	0.09–0.30	0.18–0.20	1.1–1.2	2650	0.8–2.7					
Glass sphere (WS)	0.36–0.71	0.96	[2.7]	2500	3.1–6.1					
Snow	0.48	0.3	1.5	910	2.1					
Mustard seed	1.80	0.51	1.5	1670	9.4					
Ice particle	2.80	0.35–0.65	1.0–1.9	910	8.0					
	α_E	V_E ($m\,s^{-1}$)	V_E/u_*	V_{3E} ($m\,s^{-1}$)	V_{3E}/u_*	V_{1E} ($m\,s^{-1}$)	V_{1E}/u_*			
Snow (AM)	49	1.04	3.3	0.48	1.6	—	—			
Sand (WR)	21–33	2.16–2.40	5.8	0.82	2.1	—	—			
Sand (NHB)	34–41(19)	0.76–0.88	3.5–4.4	0.39–0.43	2.0	—	—			
Glass sphere (WS)	50	0.69	0.7	⟨0.5⟩	⟨1.3⟩	—	—			
Snow	25(15)	0.87(0.42)	2.9	0.34(0.22)	1.1	0.77(0.42)	2.6			
Mustard seed	23(18)	1.1(0.8)	2.1	0.30(0.23)	0.59	1.00(0.72)	2.0			
Ice particle ($u_* = 0.65\,m\,s^{-1}$)	21(15)	1.6(1.2)	2.5	0.51(0.44)	0.78	1.52(1.18)	2.3			
	α_I	V_I ($m\,s^{-1}$)	V_I/u_*	V_{3I} ($m\,s^{-1}$)	V_{3I}/u_*	V_{1I} ($m\,s^{-1}$)	V_{1I}/u_*	V_I/V_E	V_{3I}/V_{3E}	$\alpha E/\alpha_I$
Snow (AM)	11	1.9	6.3	0.37	1.25	—	—	1.8	0.78	2.5
Sand (WR)	9.6–12.7	3.50–3.94	9.0–10.0	0.38	0.99	—	—	1.6	0.47–0.86	2.0–4.2
Sand (NHB)	11–14	1.30–1.50	7–7.3	0.21–0.31	1.2–1.5	—	—	1.6–2	0.53–0.73	2.6–3.2
Glass sphere (WS)	13.9	1.60	1.7	—	—	—	—	2.3	0.73	3.6
Snow	11(6)	1.5(1.1)	5.0	0.26(0.19)	0.87	1.4(1.1)	7.0	1.7	0.76	2.3
Mustard seed	12(7)	1.7(1.3)	3.4	0.30(0.19)	0.59	1.7(1.0)	3.3	1.6	1.00	1.9
Ice particle ($u_* = 0.65\,m\,s^{-1}$)	10(5)	2.5(1.6)	3.8	0.39(0.29)	0.60	2.4(1.6)	3.7	1.5	0.76	2.1

TABLE 3. The mean values of saltation trajectory statistics. AM, Araoka & Maeno (1981); WR, Willetts & Rice (1985); NHB, Nalpanis, Hunt & Barrett (1993); White & Schulz (1977). All values denote the mean values and value in parenthesis shows the standard deviation. [ ]: calculated by Bagnold's equation. ⟨ ⟩: estimate.

Ejection

u_* ($m\,s^{-1}$)	u_*/u_{*t}	α_E	V_E ($m\,s^{-1}$)	V_E/u_*	V_{3E} ($m\,s^{-1}$)	V_{3E}/u_*	V_{1E} ($m\,s^{-1}$)	V_{1E}/u_*
0.35	1.0	18(13)	1.9(1.0)	5.4	0.50(0.3)	1.4	1.82(1.0)	5.2
0.50	1.4	20(13)	1.8(1.2)	3.6	0.55(0.7)	1.1	1.70(1.1)	3.4
0.65	1.9	21(15)	1.6(1.2)	2.5	0.51(0.4)	0.78	1.52(1.2)	2.3

Impact

u_* ($m\,s^{-1}$)	α_I	v_I ($m\,s^{-1}$)	V_I/u_*	V_{3I} ($m\,s^{-1}$)	V_{3I}/u_*	V_{1I} ($m\,s^{-1}$)	V_{1I}/u_*	V_I/V_E	v_{3I}/V_{3E}	α_E/α_I
0.35	18(8)	1.8(0.8)	5.1	0.48(0.2)	1.4	1.7(0.8)	4.9	0.95	0.96	1.0
0.50	14(6)	2.3(1.4)	4.6	0.50(0.4)	1.0	2.2(1.4)	4.4	1.3	0.91	1.4
0.65	10(5)	2.5(1.6)	3.8	0.39(0.3)	0.6	2.4(1.6)	3.7	1.5	0.76	2.1

TABLE 4. Statistics of ice particle saltation trajectories over a range of wind speeds. Value in parenthesis shows the standard deviation. (The quantities are mean values unless otherwise stated.)

The mean normalized resultant ejection speed ($\langle V_E\rangle/u_* = 2.9$) and mean vertical speed ($\langle V_{3E}\rangle/u_* = 1.1$) for the snow particles ($d = 0.48$ mm) also lie in the same range as other studies. But, for the larger mustard seeds and ice particles, $\langle V_E\rangle/u_*$ and $\langle V_{3E}\rangle/u_*$ are significantly less than the values for small particles, by about 30%–50%. Note that for these cases the horizontal and vertical velocities of the particles are comparable with horizontal turbulent velocity fluctuations (i.e. $\sigma_u/u_* \approx V_{1E}/u_*$) (Nalpanis 1985).

The results for impacting particles show that the angles $\langle\alpha_I\rangle$ are comparable with other results, but the velocities for higher values of u_*/u_{*t} and for the larger particles are about 50% below the values for small particles and lower u_*/u_{*t}.

The variation in these parameters with u_* as it increases from its threshold value to about $1.9u_{*t}$ is shown in table 4 for the large ice particles. Note how $\langle\alpha_E\rangle$ hardly increases, while $\langle\alpha_I\rangle$ decreases 40%. The vertical component of the particles' ejection and impact velocities relative to the turbulence, $\langle V_{3E}\rangle/u_*$ and $\langle V_{3I}\rangle/u_*$, also decreased by about 50%, and the average shape of the trajectories becomes more flat. Comparing changes of $\langle V_{3I}\rangle/u_*$ for the snow and ice particles at the same value of u_*/u_{*t} (i.e. 0.3 and 0.50 $m\,s^{-1}$ respectively) shows that this ratio increases with diameter.

The statistical properties of the frequency distributions of the ejection and impact velocities and angles have been tabulated (and are available from the authors or the JFM office in Cambridge). Significantly skewed distributions (with single peaks near the low end) with long tails (i.e. large kurtosis) are observed for all particles (as noted earlier by NHB). However, these tails being much larger for mustard seeds while the mean value of V_{3E}/V_{3I} is smaller suggests that the greater adhesiveness and non-rigidity of these particles has a significant effect on their trajectories, for example by reducing the number of ejected particles and their speed when a descending particle impacts on a bed, so that only occasional events are significant. Recent research on the statistical distribution of non-ideal solid particles in random motion shows that even quite small departures of the restitution coefficient from 1.0, lead to coalescence of particles and significantly non-Gaussian statistics (e.g. Hansen 1998).

These comparisons indicate that the dimensionless results by NHB cannot be assumed to be the same when the particle sizes are increased significantly, or, at least for certain aspects, when the nature of the particle changes (e.g. ice to mustard seeds).

The marked change in the trajectory when $u_*/u_{*t} > 1.5$ is demonstrated by mea-

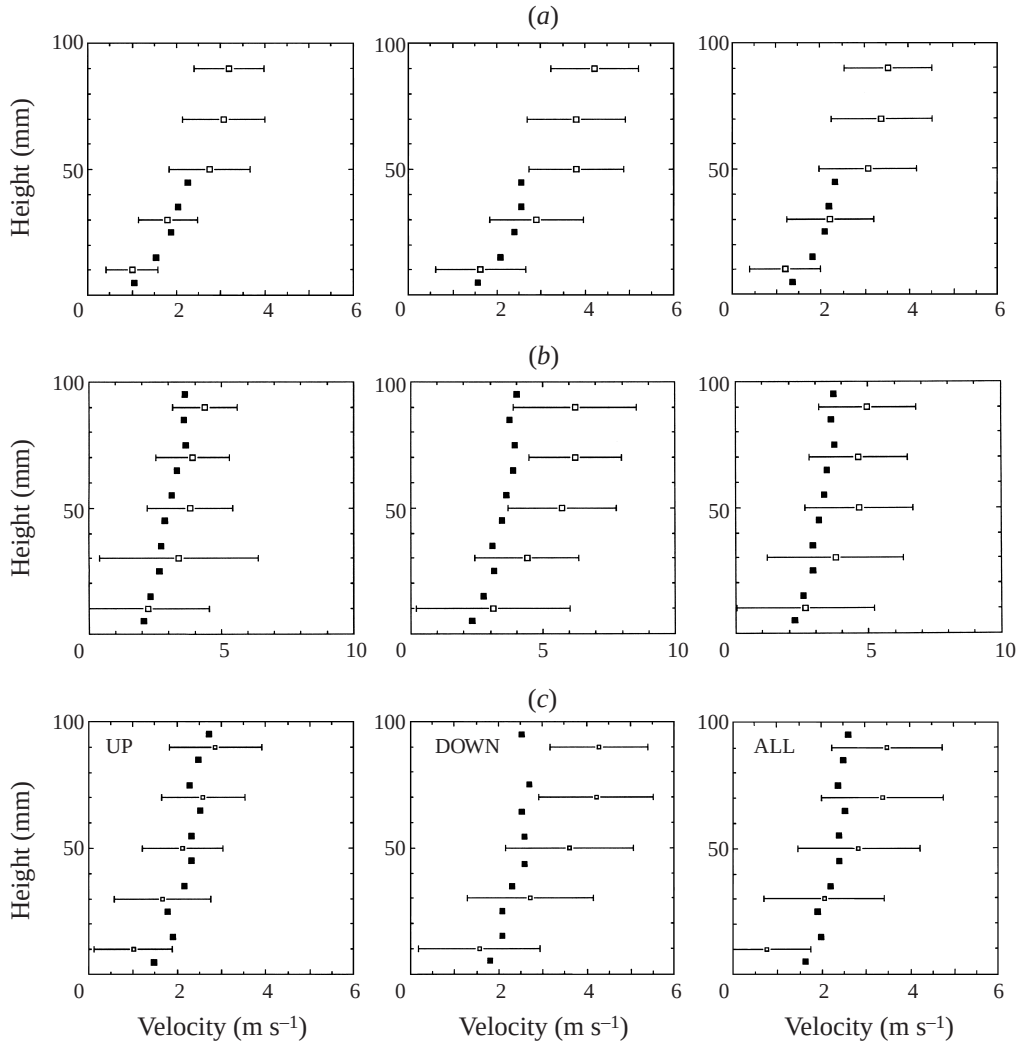

FIGURE 6. Profiles of horizontal particle velocities: (*a*) snow, friction velocity 0.30 m s^{-1} (= $1.5u_{*t}$); (*b*) Ice particles, friction velocity 0.65 m s^{-1} (= $1.9u_{*t}$); (*c*) mustard seeds, friction velocity 0.51 m s^{-1} (= $1.3u_{*t}$). Left-hand plot is for ascending particles, centre is for descending, and right-hand plot is for all particles. ■, Computations for saltating trajectories; □, measurement.

surements of the standard deviation of the horizontal particle velocities σ_{VI} as they impact on the surface. At $u_*/u_{*t} = 1.5$, figure 6(*a*) shows that σ_{VI}/V_I for rising and descending phases is about 50% and 70%, respectively, for snow particles measured at a height $z \sim 3\langle h \rangle$, where $\langle h \rangle$ is the mean rise height (estimated as 5–6 mm see table 6 below). This is quite consistent with fluctuations in the ejection velocities caused by random collisions in the bed of particles. However, figure 6(*b*) shows that σ_{VI}/V_I rises to about 120% and 100% respectively when $u_*/u_{*t} = 1.9$ for the ice particles. This cannot be explained by random collisions in the bed, but is consistent with the hypothesis that, at this higher wind speed, turbulence begins to affect the trajectories. The mustard seed particles where $u_*/u_{*t} \approx 1.5$ also demonstrate the same effect (see figure 6*c*).

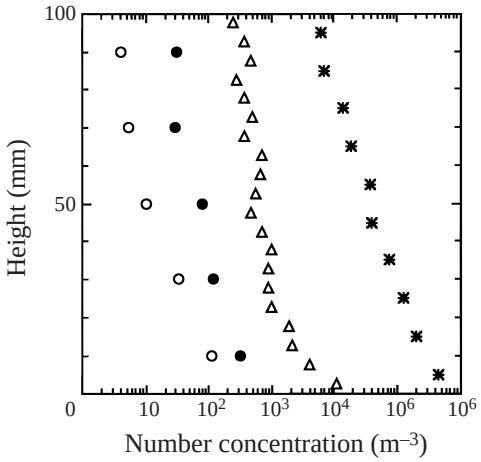

FIGURE 7. Profiles of particle number concentration: *, snow at $u_* = 0.30\,\mathrm{m\,s^{-1}} = 1.5u_{*t}$; △, mustard seed at $u_* = 0.51\,\mathrm{m\,s^{-1}} = 1.3u_{*t}$; ○, ●, ice particles at $u_* = 0.35\,\mathrm{m\,s^{-1}} = 1.0u_{*t}$ and at $u_* = 0.50\,\mathrm{m\,s^{-1}} = 1.4u_{*t}$ respectively.

3.3. *Particle concentration*

Figure 7 shows the particle concentration profiles of snow, ice particles and mustard seeds. Since all data were obtained through analysing video film, there were no experimental errors caused by any particle traps disturbing the air. Number concentrations in the saltating layer were 10^5 to $10^6\,\mathrm{m^{-3}}$ for snow, 10^2 to $10^3\,\mathrm{m^{-3}}$ for ice particles and $10^4\,\mathrm{m^{-3}}$ for mustard seeds. The average contribution to the total fluid density from the mustard seed particles from height 0 to 10 mm is less than 5%. This is presumably the reason why there was only a small effect on the mean wind profile in figure 4. The concentration decreased exponentially with increase in height (z) in all cases.

3.4. *Horizontal flux*

The horizontal flux as a function of height $f(z)$ was also obtained from the same video analysis. Further, by integrating these flux profiles a total horizontal flux per unit width F_t was calculated. As will be shown later, the flux profile of ice particles at $u_*/u_{*t} = 1.9$ did not show an exponential decay and the integration was from the surface to 100 mm which corresponds to the thickness of the boundary layer in the wind tunnel.

Based on Bagnold's (1941) arguments on the particle transport, the total horizontal flux including creep and saltation is described by a formula that is independent of the density of the particles, i.e.

$$F_t = C\sqrt{\frac{d}{d_s}}(\rho_a/g)u_*^3, \tag{3.3a}$$

where F_t is the total horizontal mass flux per unit width, ρ_a is the density of air, d is the grain diameter, d_s is the 'standard' grain diameter of 250 μm, and C is a dimensionless coefficient with the following values: 1.5 for nearly uniform sand and 2.8 for a sand of a very wide range of grain size (see also NHB's supporting argument). Substituting the appropriate values for the particles used in our experiment, the total horizontal

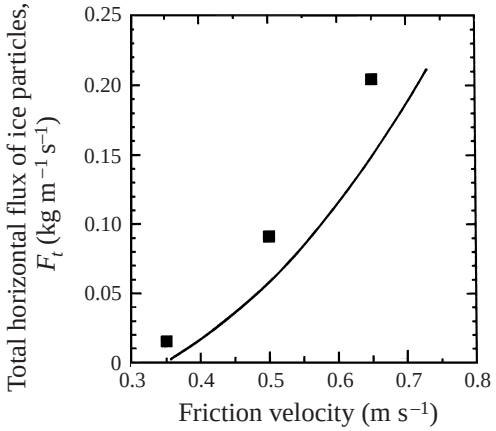

FIGURE 8. Total horizontal flux of ice particles F_t against the friction velocity. Solid line shows the prediction by Sorensen (1991).

flux of snow and ice would, according to Bagnold's estimate (3.3*a*), lie in the range

$$F_{t,snow}^{(B)} = (2.1 \sim 4.0) \times 10^{-1}(\mathrm{kg\,s^2\,m^{-4}}) \times u_*^3, \quad F_{t,ice}^{(B)} = (5.1 \sim 9.6) \times 10^{-1}(\mathrm{kg\,s^2\,m^{-4}}) \times u_*^3. \tag{3.3b}$$

Our measurements of $F_{t,ice}^{1/3}$ plotted against u_* for the ice spheres showed a linear relationship with a correlation coefficient of 0.998. A similar relationship between mass flux and u_* was observed for snow and ice particles, as follows:

$$F_{t,snow} = 4.2 \times 10^{-1}(\mathrm{kg\,s^2\,m^{-4}}) \times u_*^3, \quad F_{t,ice} = 7.5 \times 10^{-1}(\mathrm{kg\,s^2\,m^{-4}}) \times u_*^3. \tag{3.3c}$$

Considering that the size of the snow particles has a wide distribution and the ice particles are rather uniform, by comparing (3.3*b*) and (3.3*c*) we can conclude that Bagnold's expression with the same coefficient C is broadly applicable for particles with a different size, shape and density (at least for $d < 250\,\mu\mathrm{m}$; $900 \leqslant \rho_p/\rho_a \leqslant 2600$). Thus, we can reasonably say that it is largely independent of the characteristics of the particles and only depends on their diameter and probably their size distributions. Sorensen (1991) modified Bagnold's flux formula to allow for F_t being zero at the threshold value of u_* and derived an equation for the total horizontal mass flux which is also an approximately cubic function of u_*:

$$F_{t.} = 0.0014\rho_a\, u_*(u_* - u_{*t})(u_* + 7.6u_{*t} + 205) \tag{3.4}$$

He used the c.g.s. system of units for sand. In figure 8, although the measurements are slightly larger than predicted by equation (3.4), in general a similar trend is found.

Horizontal flux profiles normalized with total horizontal flux F_t are shown in figure 9(*a*) for snow, figure 9(*b*) for mustard seeds and figure 9(*c*) for ice particles. In other experiments where $u_*/u_{*t} \leqslant 1.5$ it has also been found that the flux profiles vary exponentially with height, like those of Rasmussen *et al.* (1985), Gerety (1985), Sorensen (1985), Takeuchi (1980) and White & Mounla (1991) for sand and snow. Note that for the ice particles when $u_*/u_{*t} = 1.9$, $f(z)$ is approximately constant.

NHB suggested that if there is an exponential dependence of the mass distribution f with height z, the scale height l_f (where $f(l_f) \sim (1/\mathrm{e})f(z=0)$) that determines the decay would be of the order of the mean height h to which the particles rise, i.e.

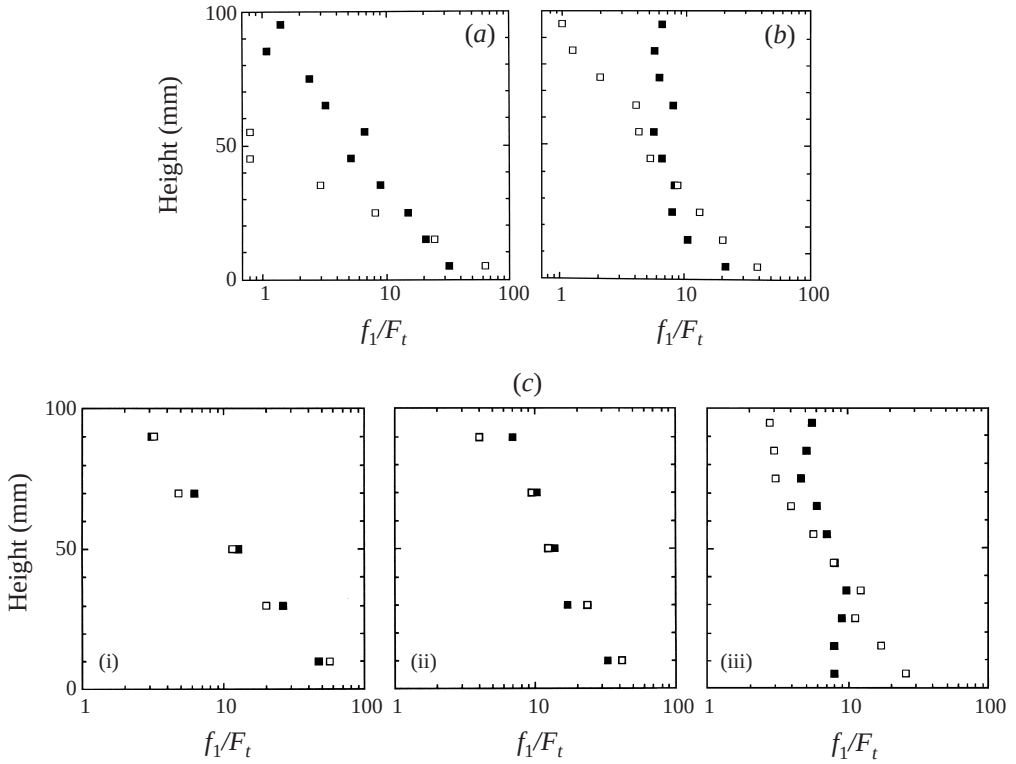

FIGURE 9. Simulated and measured horizontal fluxes of snow (*a*) ($u_* = 0.30\,\mathrm{m\,s^{-1}} = 1.5u_{*t}$), (*b*) mustard seeds ($u_* = 0.51\,\mathrm{m\,s^{-1}} = 1.3u_{*t}$), (*c*) ice particles ($u_*/u_{*t} = 1.0$ (i), 1.4 (ii), 1.9 (iii)). □, Computations; ■, measurement. Abscissa is normalized on the integrated flux, F_t.

$l_f \sim h$. Since $h \propto u_*^2/g$, it was suggested that

$$f(z) = \phi \exp(-\lambda z/(u_*^2/g)), \tag{3.5}$$

where ϕ and λ are dimensionless parameters for a single experiment. If equation (3.5) is to be consistent with equation (3.3*a*), then

$$\phi = \rho_a u_* \lambda C \sqrt{d/d_s}. \tag{3.6}$$

NHB pointed out that while this was a physically plausible scaling, in fact the value of λ was not a constant. This is probably because $h/(u_*^2/g)$ varies considerably with the diameters of the particles (typically rising as d increases which therefore indicates that λ should decrease). The values of the scaling parameter evaluated from our measured profiles (one of which is shown in figure 9*a–c*) are listed in table 5, along with values from other experiments (NHB; WS). Note that (3.7) implies that ϕ is independent of the particle density ρ_p.

White & Mounla (1991), based on their data analysis, found that λ and ϕ both increased with u_*. However, results obtained in this study show a clear decrease of λ with friction velocity. In other words, the gradient of flux decreases with an increase in friction velocity u_*. This is evident from figure 9(*b*), as well. In addition it can be deduced that particle size also has a strong effect on the flux profile parameter; it is clear in the case of snow and ice particles in table 5 that λ decreases with increasing particle size. NHB proposed (u_*^2/g) as the vertical scale height, since the

	Snow	Ice particles			Mustard seed	Sand	Walnut shell
d (mm)	0.48	2.80	2.80	2.80	1.80	0.1–0.3	0.25
u_* (m s^{-1})	0.3	0.35	0.5	0.65	0.51	0.3	–
u_*/u_{*t}	1.4	1.0	1.4	1.9	1.5	1.1–1.2	–
l_f (mm)	20	30	50	?	15		
λ	0.45	0.33	0.30	0.16	0.21	0.7–1.2	1.0–1.5
λ'	0.6	1.02	0.71	0.30	0.17	1.2–2.1	–

TABLE 5. Parameter λ of the horizontal flux profile; sand: NHB, walnut shell: WS.

vertical component of ejection velocity $\langle V_{3E} \rangle$ is nearly $2u_*$, according to both their own experiments for sand and AM's for snow. However, table 3 shows that this relation is not always universal, in particular for larger particles. Thus, in order to discuss the gradient of flux profiles obtained under different conditions more precisely, (V_{3E}^2/g) should be introduced as a measure of height instead. Then $f(z)$ is described by the expression

$$f(z) = \phi' \exp(-\lambda' z/(V_{3E}^2/g)) \tag{3.7}$$

Table 5 also shows the calculated dimensionless parameter λ' for the vertical scale height V_{3E}^2/g. It is noteworthy that λ' for ice particles decreases linearly with u_*. One has to conclude that although both exponential flux curves and the Bagnold integrated flux formula are useful approximations, there are uncertainties about the variations in the coefficient λ that are not explicable in terms of h or V_{3E}. In fact the explanation may be that there is a transition from saltation to suspension when $u_*/u_{*t} \geqslant 1.5$.

4. Simulations

4.1. *Computation of particle trajectories*

In saltating flow when the particle elevation is significantly greater than the grain diameter, i.e. $z \gg d$, the effects of lift forces and of random forces caused by turbulent eddies on a particle are negligible and the most significant forces acting on it are drag and gravity (NHB).

Then the motion of a spherical particle in a cross-wind is described by the following equations:

$$\frac{\mathrm{d}x}{\mathrm{d}t} = V_1, \tag{4.1}$$

$$\frac{\mathrm{d}z}{\mathrm{d}t} = V_3, \tag{4.2}$$

$$\frac{\mathrm{d}V_1}{\mathrm{d}t} = -\frac{3}{4}\left(\frac{\rho_a}{\rho_p d}\right) C_d V_R (V_1 - U), \tag{4.3}$$

$$\frac{\mathrm{d}V_3}{\mathrm{d}t} = -\frac{3}{4}\left(\frac{\rho_a}{\rho_p d}\right) C_d V_R V_3 - g, \tag{4.4}$$

where d is the particle diameter, ρ_a and ρ are the densities of the air and particle respectively, g is the acceleration due to gravity, U is the horizontal (x-direction wind

speed), and relative velocity V_R is written as

$$V_R = \left((V_1 - U)^2 + V_3^2\right)^{1/2}. \tag{4.5}$$

For a sphere, the drag coefficient C_d for low Reynolds number Re has been formulated by Morsi & Alexander (1972) as

$$C_d = \frac{24}{Re} + \frac{6}{1 + Re^{1/2}} + 0.4, \tag{4.6}$$

and

$$Re = dV_R/v \tag{4.7}$$

where v is the kinematic viscosity of air.

The mean wind speed U was assumed to vary vertically with a logarithmic law as in § 3.1. In natural conditions, when u_*/u_{*t} is greater than 2.0, the wind profile near the surface is likely to be modified due to the particle drag as discussed in § 3.2. However, for these experiments, where $u_*/u_{*t} < 2$ the log wind profile assumption is satisfied as shown in figure 4.

Given the initial conditions for the particle trajectory, namely the ejection velocity and angle, the trajectory of a saltating particle can be computed from the above equations. Substituting the average ejection conditions (V_{1E} and V_{3E}) listed in table 3, particle trajectories were calculated for snow, ice particles and mustard seeds. Calculated impact variables are shown in table 6. Simulated results agree fairly well with the experimental ones to within 10%. Although the calculated α_I is larger and V_I is smaller than the measured values, the results lie well within one standard deviation of the measured values. The errors may be due to the small differences between the actual velocity profile, and to the assumption that the particles are ideal spheres.

The mean rise heights $\langle h \rangle$ of trajectories were not measured in this study. However, the results of the experiments on small snow particles (0.2 mm in diameter) by AM and on sand particles by NHB are consistent with the nonlinear, non-Stokesian drag formulation of (4.3) and (4.6). They showed that there is a significant vertical drag on the particles, which reduces $\langle h \rangle$ by about 60%–40% (NHB). The same approach is used here to calculate h, normalized by the vertical kinetic energy (per unit weight) of the ejected particle $V_{3E}^2/2g$. The result in figure 10 shows clearly how $\langle h \rangle$ increases with particle size as the relative importance of drag is reduced. Thence from table 2, for large snow and ice particles $\langle h \rangle$ is about 85% to 95% of its value in still air. Note that $\langle h \rangle$ is greater in these experiments for the large ice particles than for the smaller mustard seed particles, because V_{3E}/u_* is greater.

4.2. *Mass flux modelling*

4.2.1. *Method*

By substituting the measurements of the ejection velocity into the saltation model, vertical profiles of the horizontal flux were estimated. The computing procedure consisted of three parts: definition of the particle ejection statistics (initial particle speeds and angles), trajectory modelling, and counting of particles to obtain fluxes.

In this model more than 5000 particles are ejected, from random positions in the test region chosen to be $4\langle l \rangle$ long, in which $\langle l \rangle$ is a mean saltation length as listed in table 6. Their initial velocity distribution is determined from our experiments. Figure 11 shows the relation between ejection angle α_E and velocity V_E obtained in the experiments. Although there is a wide scatter, there is a small negative trend in these figures. The correlation and covariance between them were calculated and these values

	α_I	V_I (m s^{-1})	V_I/u_*	V_{3I} (m s^{-1})	V_{3I}/u_*	V_{1I} (m s^{-1})	V_{1I}/u_*	V_I/V_E	V_{3I}/V_{3E}	h (mm)	l (mm)
Snow – exp	11(6)	1.5(1.1)	4.9	0.3(0.19)	0.9	1.4(1.1)	4.8	1.7	0.8	–	–
Snow – c	11	1.5	5.1	0.3	1.0	1.5	5.0	1.8	0.9	5.2	76
Mustard seed – exp	12(7)	1.7(1.3)	3.4	0.3(0.19)	0.6	1.7(1.0)	3.3	1.6	1.0	–	–
Mustard seed – c	13	1.2	2.4	0.3	0.6	1.2	2.4	1.2	1.0	4.5	66
Ice sphere – exp	10(5)	2.5(1.6)	3.8	0.4(0.29)	0.6	2.4(1.6)	3.7	1.5	0.8	–	–
Ice sphere – c	12	2.3	3.6	0.5	0.7	2.3	3.5	1.5	0.9	12.8	190

TABLE 6. Particle trajectory simulation results. exp: experiment, c: numerical simulation. For input data of V_{1E} and V_{3E}, see table 3. Brackets in experimental data denote the value of the standard deviation.

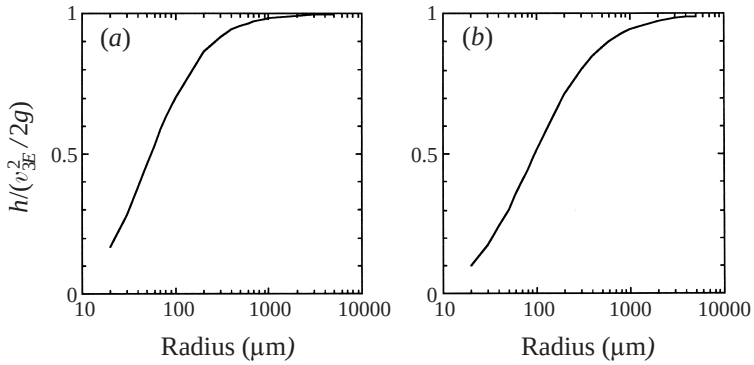

FIGURE 10. Variations of the normalized maximum rise height of saltating particles with particle diameter. (*a*) $V_{3E} = 0.34\,\mathrm{m\,s^{-1}}$, $V_{1E} = 0.77\,\mathrm{m\,s^{-1}}$, $u_* = 0.30\,\mathrm{m\,s^{-1}}$ (initial condition for snow in table 3), (*b*) $V_{3E} = 0.51\,\mathrm{m\,s^{-1}}$, $V_{1E} = 1.52\,\mathrm{m\,s^{-1}}$, $u_* = 0.65\,\mathrm{m\,s^{-1}}$ (initial condition for ice particles in table 3).

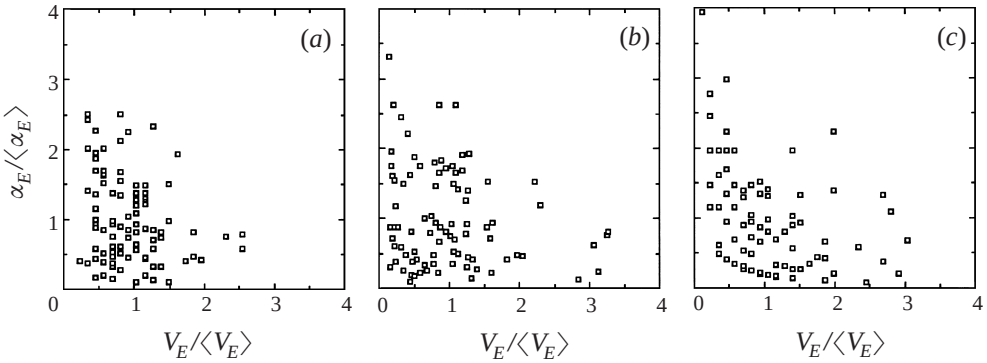

FIGURE 11. Relation between normalized ejection angle α_E and velocity V_E obtained in the experiments: (*a*) snow, covariance and correlation are −0.666 and −0.229 respectively ($u_*/u_{*t} = 1.5$); (*b*) ice particles, −0.115 and −0.226 ($u_*/u_{*t} = 1.9$); (*c*) mustard seeds, −0.263 and −0.375 ($u_*/u_{*t} = 1.3$).

were used to generate a two-dimensional joint-normal random number distribution. Initial velocities and angles used in the simulation are shown in figure 12.

The trajectory model introduced in § 4.1 was used in the calculation. Trajectories were continued until the particle either passed through 'numerical traps' or impacted on the surface. Numerical traps were set up to count particles passing a certain point at a given height. They were analogous to the physical traps used in conventional experiments and field measurements in which a series of traps are placed at the downwind end of a particle bed (e.g. Bagnold 1941). Calculations were performed for the mean diameter of each sample: size distribution was not taken into account.

The above computing procedures were practically the same as proposed by NHB but the input data differed, being based on the new measurements reported here.

4.2.2. *Results and comparison with experiments*

Computations of the horizontal flux profiles normalized on total horizontal flux for snow, mustard seeds and ice particles are shown in figures 9(*a*), 9(*b*) and 9(*c*) respectively and compared with profiles obtained in the wind tunnel experiments. For $u_*/u_{*t} \leqslant 1.5$ an exponential decay of the flux with height was obtained in all cases

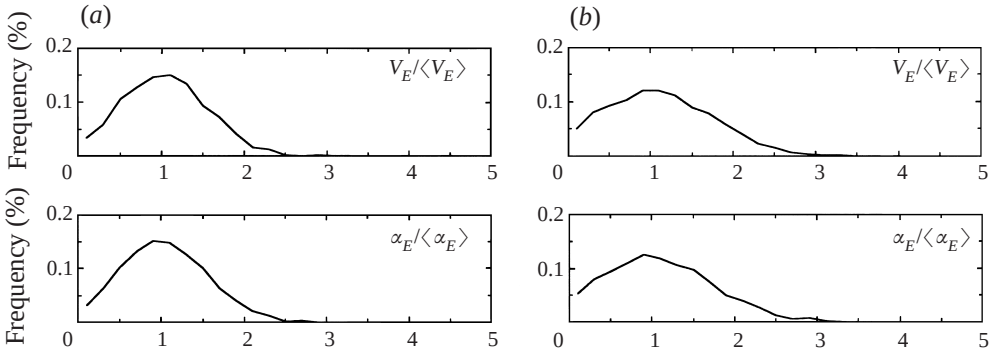

FIGURE 12. Distribution of ejection velocities and angles generated with a two-dimensional joint-normal random number distributions and used in the flux simulation: (*a*) snow ($u_*/u_{*t} = 1.5$), (*b*) ice particles ($u_*/u_{*t} = 1.9$).

and it supports the basic validity of this model. For the mustard seeds ($u_*/u_{*t} \approx 1.5$) the profile changes its form at a height of $z \approx 10\langle h\rangle$ to become nearly uniform with height.

Simulations in figure 9(*c*) show how the parameter λ for the flux decay with height varies with friction velocity u_* and particle size. The results indicate the same trend as noted in table 5 namely that λ decreases as u_*/u_{*t} increases. The computations and experiments for ice particles at $u_*/u_{*t} = 1.0$ and 1.4 agree well. Note that the agreement of the simulated profiles, when normalized, with (3.6) in the saltation regime implies that the rate of ejection of particles from the surface is inversely proportional to the particle density ρ_p, although their velocity of ejection is independent. For the ice particles at the higher wind speed $u_* = 0.65\,\mathrm{m\,s^{-1}}$ ($\approx 1.9\,u_*$) the profiles are quite different and are almost constant with height. This suggests that the particle motions are then in a different regime.

5. Discussion and conclusion

The results presented here for wind tunnel measurements of the trajectories of particles of different size and density in a turbulent wind of varying velocity appear to cover the regimes of both saltation and transition to suspension.

The trajectories, and ejection and impact velocities of the particles were recorded and analysed, even those that rose only about one diameter into the flow. That is why the means and variances of these velocities, when normalized on u_*, although similar to those measured in previous experiments on saltating particles, are about 20% lower. As shown in table 3, with increasing particle size the ejection angle and the normalized ejection velocity V_E/u_* and its horizontal component V_{1E}/u_* decreased. By contrast the impact angle and its horizontal velocity component V_{3I}/u_* and V_{1I}/u_* increased. It is noteworthy that the values of V_{3E}/u_* are identical in both experiments. Thus a useful working hypothesis is that V_{3E} is proportional to the friction velocity and does not vary with the grain size. Note that the sphericity of snow particles is less than those of ice and mustard seed particles and the size distribution is much broader than those of ice particles. In fact, the kurtosis of ejection angles and of velocities for snow are generally smaller values than for ice particles. This is probably caused by the differences in shape and size distribution.

The effects of particle density on the saltation trajectory could not be studied here independently of the more significant effects of friction velocity and particle size. The main effect as shown in figure 10 is that the larger particles could rise higher (for given initial velocity). The restitution coefficient is also an important factor because the skewness and kurtosis of the velocity statistics of the mustard seeds are up to a factor of 2 greater than those for other particles, as explained in § 3.2.

However, this study has confirmed previous findings about the main features of the saltation regime for a wide range of sizes, shapes and density of particles, even when the particles are not ideal, as with the mustard seeds used here which have a coefficient of restitution of only 0.7. The most important practical finding is that the formulae for the flux profile (3.6) and the total flux (3.4) are generally applicable in the saltation regime. Since snow and sand have fairly wide size distributions in nature, this hypothesis about the general occurrence of the main features of saltation found here is of considerable environmental and practical significance. Even so, within the saltation regime, there are interesting variations in the statistics of the particle motion according to the size, type and distribution of particles. These need to be further examined. Recently a snow particle counter, which can sense not only the number of particles but also their diameters, has been developed (Kimura, Maruyama & Ishimaru 1993). Since experiments using this device are expected to provide trajectories more readily, concentrations and flux as a function of particle diameter and density more progress can be expected in understanding the dependence of the saltation statistics on the particle size distribution and type of particle.

Another aspect of the saltation mechanism that is still not well understood is the effect of the particles' momentum on the mean velocity profile (McEwan & Willetts 1993). Although Bagnold (1941) found a significant change in the logarithmic profile below the mean height of the particle trajectories, in these and other wind tunnel experiments, and although the momentum flux of the particles ($\propto \rho_p C V_1^2$) is comparable to that of the air flow ($\propto \rho_a u^2(z = h)$), the modification of the wind profile caused by the particle drag was negligible for a near threshold case. The change in the eddy structure of the turbulent boundary layer near the ground, from being driven 'bottom up' to 'top down' when $u_* h/\nu \geqslant 10^5$ may explain this difference, based on the recent work of Hunt & Morrison (2000).

When $u_*/u_{*t} = 1.5$, the results show (as anticipated by Owen's 1964 physical arguments and Nalpanis's 1985 simulations) that the turbulent velocities distort the particle trajectories. We see this first in the upper part of the flux curve when $u_*/u_{*t} \geqslant 1.5$ and then in the whole flux curve when $u_*/u_{*t} = 1.9$. This implies that the trajectories and the velocity fluctuations of the particles (e.g. σ_{V3}) become progressively more random as the wind speed increases. One demonstration of this is the increase of σ_{VI}/V_I from 0.5–0.7 when $u_*/u_{*t} < 1.5$, to 1.0 when $u_*/u_{*t} \approx 1.9$ near the surface and even more at higher levels where $z \sim \langle h \rangle$ (figure 6*b*). This explains the change in the flux curves and probably the reduction in the coefficient of λ in equation (3.5) (for a given type of particle). These trends have been described before, although systematic measurements have not previously been performed.

The above criterion for the transition from saltation to the suspension regime can be explained more precisely than by Owen (1964) and Nalpanis (1985) by considering how the particles are displaced randomly from the parabolic saltation trajectories by the random drag forces acting on them by the turbulent eddies. Near the top of the trajectories, when the particles are moving nearly horizontally with a velocity (V_1, V_3), V_1 differs from the mean velocity U_1 by about $\pm U_1/2$, while V_3 is approximately zero. Using the nonlinear drag law discussed by NBH, the vertical

acceleration caused by a vertical gust u_3' is of order

$$\frac{\mathrm{d}V_3}{\mathrm{d}t} \sim \left(\frac{\rho_a}{\rho_p}\right) \frac{u_3' U_1(h)}{4a},$$

where

$$U_1(h) \approx \frac{u_*}{\kappa} \ln\left(\frac{h}{z_0}\right).$$

Thence over the period T_p of the saltation trajectory, since

$$T_p \sim \frac{12h}{V_{1I}} \approx \frac{10h}{4u_*},$$

$$V_3 \sim \left(\frac{\rho_a}{\rho_p}\right) \frac{10u_3' h}{4a} \left(\frac{\ln(h/z_0)}{4\kappa}\right) \sim \left(\frac{\rho_a}{\rho_p}\right) 15u_3' \left(\frac{u_*^2}{2ga}\right)$$

Therefore, from § 3.1.1

$$\frac{u_*}{u_{*t}} \sim \frac{1}{\sqrt{22}} \left(\frac{V_T}{u_{*t}}\right) \sim 4.$$

This is of the same order as our observed values. In our case for $u_*/V_T \sim 1/10, u_*/u_{*t} \sim 1.5$ to 2.0 when the transition begins.

Thus even when the fall speed (in still fluid) is four times greater than the typical vertical velocity of the turbulence, the turbulence has a significant effect on the parabolic trajectories of the particles and thence on the mean fall speed of the descending particles. By comparison, when particles settle in turbulent flow away from boundaries, when $V_T/u_3' \sim 4$, there is no effect on the mean fall speed (e.g. Srdic 1998; Davilla & Hunt 1999).

There are two main hypotheses about the behaviour of particles near the bed when $u_*/u_{*t} = 1.5$. The first, two-layer hypothesis is that, as we see in figure 9(*b*), there would continue to be a saltation layer near the surface beneath a deeper layer of suspended particles. This would imply that the ejection process would continue to be controlled by collision with impacting particles, and therefore that the ratio of V_{3I} to V_E should remain approximately constant, and in particular that V_E should remain greater than the typical horizontal velocity fluctuations ($\sim 2.5u_*$). Table 4 shows quite clearly that these conditions are not satisfied.

The second, one-layer, hypothesis is that, as u_*/u_{*t} increases, the particle motion is controlled by turbulence right down to the surface and that it is aerodynamic forces on the particles caused by the mean flow and the eddies that lift them (e.g. Reeks, Reed & Hall 1988). In that case the typical vertical velocity V_{3E} should be equal to or less than the r.m.s. turbulent velocity ($\sim 1.3u_*$) depending on the weight of the particle. (Note that lift forces also produce a contribution to V_{3E} of this order because they act over a period comparable with the relaxation time of the particle ($\tau_p \sim d(\rho_p/\rho_a)/u_*$).) The horizontal component of the velocity V_{1E} is now comparable with $\sigma_u \sim 2.5u_*$. These estimates for V_{3E} and V_{1E} are consistent with the trend of the data as u_*/u_{*t} increases.

A further implication of this one-layer hypothesis concerns particle trajectories near the surface where the time scale of the vertical component of the turbulent eddies $T_L(z)$ is of the order of $\frac{1}{2}(z/u_*)$, and therefore decreases near the surface (e.g. Hunt & Weber 1979). This means that below a level $z_p \sim \tau_p u_* \sim 2(\rho_p/\rho_a)d$, (say 0.1–1 m for sand particles in the atmosphere), the particles travel in nearly straight lines because their inertia prevents them from following the smallest fluid eddy motion. These

trajectories can be mistaken for those produced by saltation. Therefore the particle velocities reaching the surface are determined by the mean flow and turbulence at this level. In a small-scale experiment, such as ours, the particle relaxation time is always greater than that of the turbulence, and the velocity fluctuation of the particles are of order $(T_L/\tau_p)(\sigma_w, \sigma_u)$ (see for example, Wang & Stock 1993), which in this case is of order $\frac{1}{2}(\sigma_w, \sigma_u)$. This is consistent with the reduced value of V_{3F}/u_* given in table 4.

In reality, even for much larger values of u_*/u_{*t}, the occasional impact of particles still contributes to the ejection process and also tends to reduce any adhesion of the particles. In the limit of $u_*/u_{*t} \geqslant 10$, when the vertical component of the turbulence on the surface is greater than the fall speed of the particles, the surface of the bed ceases to be well defined, and it becomes a fluidized bed.

The above hypothesis has been framed for particles which are, approximately, all of one size. When particle sizes vary, the impact of large particles leads to the ejection of smaller particles and this may be a more effective process for the suspension of smaller particles than aerodynamic processes (e.g. Eames & Dalziel 2000). Then the value of u_*/u_{*t} for the transition from collisions to aerodynamically determined ejection is higher for polydisperse particle distributions. But this concept needs further examination.

It appears that there may now be some scientific justification for the imagery used by the Arabic writer quoted by Ondaatje (1992) in his book '*The English Patient*' (published by Knopf) (which incidentally refers to Bagnold and his exploits), in describing his observations of the surface during a sand storm when obviously u_*/u_{*t} was quite large!

> It is as though the surface were underlaid with steam-pipes, with thousands of orifices through which tiny jets of steam are puffing out. The sand leaps in little spurts and whirls. Inch by inch the disturbance rises as if the desert were rising in obedience to some upthrusting force beneath. Larger pebbles strike against the skins, the knees, the thighs. The sand-grains climb the body till it strikes the face and goes over the head. The sky is shut out, all but the nearest objects fade from view, the universe is filled.

The authors gratefully acknowledge the useful suggestions and comments by Dr M. Sorensen and Dr K. R. Rasmussen of the University of Aarhus, Denmark, Professor B. B. Willetts and Dr I. K. McEwan of the University of Aberdeen, Scotland. Thanks are also due to Dr R. Perkins and Dr I. Eames of the University of Cambridge for valuable and helpful advice. The authors are grateful for support while this work was written up: K.N. to the Japan Society for the Promotion of Science for partially funding his stay at the Department of Applied Mathematics and Theoretical Physics of the University of Cambridge, and J.C.R.H. to CERFACS Toulouse and Institute Mechanique des Fluides de Toulouse.

REFERENCES

Absil, F. G. J. & Beugeling, G. L. H. 1984 The entrainment of small particles by a turbulent spot. *Proc. IUTAM Symp. on Atmospheric Dispersion of Heavy Gases and Small Particles* (ed. G. Oom & H. Tenneka), pp. 211–220. Springer.

Anderson, R. S. 1989 Saltation of sand: A qualitative review with biological analogy. *Proc. R. Soc. Edin.* B **96**, 149–165.

Anderson, R. S. & Haff, P. K. 1988 Simulation of aeolian saltation. *Science* **241**, 820–823.

Anderson, R. S. & Haff, P. K. 1991 Wind modification and bed response during saltation of sand in air. *Acta Mech.* (*Suppl.*) **1**, 21–52.

Anderson, R. S., Sorensen, M. & Willetts, B. B. 1991 A review of recent progress in our understanding of aeolian sediment transport. *Acta Mech. (Suppl.)* **1**, 1–19.

Araoka, K. & Maeno, N. 1978 Measurement of restitution coefficient of ice. *Low Temp. Sci.* A **36**, 55–65 (in Japanese with English Summary).

Araoka, K. & Maeno, N. 1981 Dynamical behaviour of snow particles in the saltation layer. In *Proc. 3rd Symp. on Polar Met. & Glaciology. Mem. Natl Inst. Polar Res., Tokyo* **19**, pp. 253–263.

Bagnold, R. A. 1941 *The Physics of Blown Sand and Desert Dunes*, Methuen.

Davilla, J. & Hunt, J. C. R. 1999 Settling of particles near vortices and in turbulence. (Submitted)

Eames, I. & Dalziel, S. B. 2000 Dust resuspension by the flow around an impacting sphere. *J. Fluid Mech.* **403**, 305–328.

Gerety, K. M. 1985 Problems with determination of u_* from wind-velocity profiles measured in experiments with saltation. In *Proc. Intl Workshop on the Physics of Blown sand* (ed. O. E. Barndorff-Nielsen), vol. 2, pp. 271–300. Mem. 8. University of Aarhus, Denmark.

Hansen, J. P. 1998 Study of random particle motion. In *Turbulence and determinism* (ed. M. Lesieur), Grenoble Sciences, Grenoble.

Hunt, J. C. R. & Morrison J. F. 2000 Eddy structure of the turbulent boundary layer. *Eur. J. Mech.* (submitted).

Hunt, J. C. R. & Weber, A. H. 1979 A Lagrangian statistical analysis of diffusion from a ground-level source in a turbulent boundary layer. *Q. J. R. Met. Soc.* **105**, 423–443.

Iversen, J. D. & White, B. R. 1982 Saltation threshold on Earth, Mars and Venus. *Sedimentology* **28**, 111–119.

Janin, L. F. & Cermak, J. E. 1988 Sediment-laden velocity profiles developed in a long boundary-layer wind tunnel. *J. Wind Engng Indust. Aerodyn.* **28**, 159–168.

Jensen, N. & Franck J. 1965 *Model Scale Wind Tunnel Tests.* Copenhagen University Press.

Kimura, T., Maruyama, T. & Ishimaru, T. 1993 SPC-III no sekkei to seisaku. *Proc. Cold Region Technology Conf. '93*, pp. 665–670. (in Japanese).

Kosugi, K., Nishimura, K. & Maeno, N. 1992 Snow ripples and their contribution to the mass transport in drifting snow. *Boundary-Layer Met.* **59**, 59–66.

McEwan, I. K. & Willetts, B. B. 1991 Numerical model of the saltation cloud. *Acta Mechanica Suppl.* **1**, 53–66.

McEwan, I. K. & Willetts, B. B. 1993 Adaptation of the near-surface wind to the development of sand transport. *J. Fluid Mech.* **252**, 99–115.

Maeno, N., Araoka, K., Nishimura, K. & Kaneda, Y. 1979 Physical aspects of the wind-snow interaction in blowing snow. *J. Fuc. Sci., Hokkaido Univ. VII* **6**, 126–141.

Morsi, S. A. & Alexander, A. J. 1972 An investigation of particle trajectories in two-phase flow systems. *J. Fluid Mech.* **55**, 193–208.

Nalpanis, P. 1985 Saltating and suspended particles over flat and sloping surfaces. II. Experiments and numerical simulations. In *Proc. Intl Workshop on the Physics of Blown Sand* (ed. O. E. Barndorff-Nielsen), vol. 1, pp. 37–66. Mem. 8, University of Aarhus, Denmark.

Nalpanis, P., Hunt, J. C. R. & Barrett, C. F. 1993 Saltating particles over flat beds. *J. Fluid Mech.* **251**, 661–685.

Owen, P. R. 1964 Saltation of uniform grains in air. *J. Fluid Mech.* **20**, 225–242.

Owen, P. R. & Gillette, D. 1985 Wind tunnel constraint on saltation. In *Proc. Intl Workshop on the Physics of Blown Sand* (ed. O. E. Barndorff-Nielsen), vol. 2, pp. 253–270. Mem. 8. University of Aarhus, Denmark.

Rasmussen, K. R., Sorensen, M. & Willetts, B. B. 1985 Measurement of saltation and wind strength on beaches. In *Proc. Intl Workshop on the Physics of Blown Sand* (ed. O. E. Barndorff-Nielsen), vol. 2, pp. 301–325. Mem. 8. University of Aarhus, Denmark.

Reeks, N. W., Reed, J. & Hall, D. 1988 On the resuspension of small particles by a turbulent flow. *J. Phys.* D **21**, 574–589.

Sorensen, M. 1985 Estimation of some aeolian saltation transport parameters from transport rate profiles. In *Proc. Intl Workshop on the Physics of Blown Sand* (ed. O. E. Barndorff-Nielsen), vol. 1, pp. 141–190. Mem. 8. University of Aarhus, Denmark.

Sorensen, M. 1991 An analytic model of wind-blown sand transport. *Acta Mechanica Suppl.* **1**, 67–82.

Spies, P.-J., McEwan, I. K. & Butterfield, G. R. 1995 On wind velocity profile measurements taken in wind tunnels with saltating grains. *Sedimentology* **42**, 515–521.

Srdic, A. 1998 Interaction of dense particles with stratified and turbulent environment. PhD thesis, Mechanical and Aerospace Engineering, Arizona State University.

Takeuchi, M. 1980 Vertical profile and horizontal increase of drift-snow-transport. *J. Glaciol.* **26**, (94), 481–492.

Townsend, A. A. 1976 *Structure of Turbulent Shear Flow*. Cambridge University Press.

Wang, L. D. & Stock, D. E. 1993 The dispersion of heavy particles by turbulent motion. *J. Atmos. Sci.* **50**, 1897–1913.

Weng, W. S., Hunt, J. C. R., Carruthers, D. J., Warren, A., Wiggs, G. F. S., Livingstone, I. & Castro I. 1991 Air flow and sand transport over sand-dunes. *Acta Mechanica Suppl.* **2**, 1–22.

Werner, B. 1990 A steady state model of wind-blown sand transport. *J. Geol.* **98**, 1–17.

White, B. R. & Mounla, H. 1991 An experimental study of Froude number effect on wind-tunnel saltation. *Acta Mechanica Suppl.* **1**, 145–157.

White, B. R. & Schulz, J. C. 1977 Magnus effect in saltation. *J. Fluid Mech.* **81**, 497–512.

Willetts, B. B. & Rice, M. A. 1985 Intersaltation collisions. In *Proc. Intl Workshop on the Physics of Blown Sand* (ed. O. E. Barndorff-Nielsen), vol. 1, pp. 83–100. Mem. 8. University of Aarhus, Denmark.